Incandescent Porous Carbon Microspheres to Light up Cells: Solution Phenomena and Cellular Uptake

Paul Duffy[a], Luís M. Magno[b], Rahul Yadav[c], Selene K. Roberts[c], Andrew D. Ward[c], Stanley W. Botchway[c], Paula E. Colavita[a]* and Susan J. Quinn[b]*

Carbon based materials are attractive for biological applications because of their excellent biocompatibility profile. Porous carbons with high specific surface area are particularly interesting because it is possible in principle to leverage their properties to deliver high drug payloads. In this work, porous carbon microspheres with high specific surface area were prepared and studied in solution and in cells. Raman optical tweezer trapping of microspheres, excited by 532 nm, results in graphitization and incandescence in solvents that display poor heat conduction. Fluorescence confocal microscopy imaging was used to demonstrate the uptake of fluorescently labelled microspheres by cells and the ability to leverage their optical absorptivity in order to cause carbon graphitization and cell death.

Introduction

Porous materials in the form of micro- and nanoparticles hold great promise as cellular delivery and imaging agents. High specific surface area and small pore sizes, in principle, allow the capture and delivery of small molecules for a variety of applications, from therapeutics to contrast agents. Mesoporous particles based on inorganic scaffolds such as silica,[1-3] zirconia[4] and infinite coordination polymers[5] have been the subject of intense investigation towards their biological application. By comparison, mesoporous carbon materials have received less attention, despite the fact that these could offer important advantages compared to their inorganic counterparts.

Carbon is in general well tolerated in vivo and is already used as a coating in biodevices and implants.[6, 7] The interaction of carbon nanoparticles with biomolecules and cells is of great interest because of both the chemical inertness of carbon and the possibility of robust surface functionalization that allows optimization of their delivery and imaging properties.[8, 9] Nanostructured carbons such as nanotubes[10] and fullerenes[11] and, more recently, carbon dots[12] and nanodiamonds[13-15] have been successfully used as intracellular delivery agents. These previous studies confirm that carbon materials display numerous advantages for this purpose. However, to our knowledge there are only two reports of cellular uptake of mesoporous carbon materials in which their high loading capacity is leveraged.[16, 17]

In this paper we investigate the properties of porous carbon microspheres of narrowly dispersed size for cell uptake and imaging. These particles display high specific surface area for delivery applications and are strong absorbers in the visible range. We present findings from combined Raman and optical tweezer studies aimed at determining and exploiting the optical properties of carbon for remote thermal triggering/activation events. Single particle studies in different media suggest that the heat dissipation properties of the medium are critical in determining the behaviour of individual particles under irradiation. Using confocal fluorescence microscopy we show that these particles are effectively internalised by cells and that laser irradiation can be used to disrupt cellular structures.

Experimental Section

Carbon microsphere preparation

Carbon microspheres were synthesized via ultraspray pyrolysis (USP) following reported methods.[18] Briefly, a 1.65 MHz piezoelectric crystal placed at the bottom of a flask was used to generate a mist from a 1 M aqueous solution of either Lithium or Sodium dichloroacetate. The mist was carried by a flow of Ar into a tube furnace, where the organic salt was pyrolyzed at 700 °C. Particles were collected in a bubbler containing deionised water, filtered and washed with copious amounts of water prior to further characterisation.

For functionalisation experiments, particles were suspended in water and refluxed in 5 M nitric acid for 2 h, then filtered and washed with copious amounts of water. Particles were then coupled to 6-aminofluorescein using a water soluble carbodiimide coupling agent (EDC) according to standard procedures.[19] The free 6-aminofluorescein was separated from 6-aminofluorescein coupled particles by repeated centrifugation and washing. For surfactant studies we prepared suspensions of pristine carbon microspheres in 0.04% solutions of N-[1-(2,3-dioloeyl)propyl]-N,N,N-trimethylammonium chloride (DOTAP) and in 1% Sodium Lauryl sulfate (SDS) solutions in deionized water. Both surfactant concentrations were above the critical micelle concentration.

Particle characterization

Scanning Electron Microscopy (SEM) was carried out on Zeiss Ultra Plus microscope using the In-lens detector. Particle size distributions were obtained via SEM from particle diameter determination of 125 and 58 particles for LiDCA and NaDCA samples. ζ-potential measurements were carried out on a Malvern

Zetasizer Nano-ZS: HCl or NaOH was added to particle suspensions in order to vary the pH followed by an addition of NaCl in order to bring the total ionic strength to a value of 0.010 M. The specific surface area of carbon spheres was determined via Brunauer-Emmett-Teller (BET) analysis (Quantachrome Nova Station).[20] The sample was pre-treated at 30 °C under vacuum for 24 h prior to analysis using nitrogen as the adsorbing gas. The specific surface area was calculated using a multi-point BET plot over relative pressures in the range 0.08-0.3. Pore size was determined via the Barrett−Joyner−Halenda (BJH)[21] method using the desorption branch of adsorption isotherms;[22] values reported represent the mode of the pore size distribution. Fluorescence (photoluminescence) spectra were measured on a Varian, Cary Eclipse fluorescence spectrophotometer at λ_{exc} = 480 nm (room temperature).

Cell cultures

Human embryonic kidney (HEK293) and human epithelial carcinoma (HeLa) cells were purchased from Prochem (EACCC, UK) and cultured under the following conditions: cells were cultured in Eagle's minimal essential media (EMEM) supplemented with 10% Foetal calf serum - (American, Fetal), 2 mM L-glutamine, 100 units/mL penicillin G sodium and 100 µg/ml streptomycin. The cells were grown by incubating at 37 °C with 5% CO_2 in humidified air until the culture reached 70% confluency before replating at 2×10^5 cells/dish, in 35 mm glass bottom dishes (MatTek Corporation, USA) containing 2-3 mL of medium prior to confocal imaging. 14 h later membrane dye labelled cells were prepared by culturing in the presence of 200 µL of 1µM 1,1'-Dioctadecyl-3,3,3',3'-tetramethylindocarbocyanine iodide (DiI, Invitrogen) in serum-free EMEM media for 8 min at 37 °C with 5% CO_2. Aqueous microsphere suspensions (0.04 mg/mL) were prepared using sterile water. The particles (50 µL) were then added to 200 µL OptiMem I reduced serum media and to this 12 µL of FuGENE®, a cationic lipid transfection agent, was added directly into the solution and mixed. After incubation for 20 min this mixture was added to cells and incubated overnight at 37 °C. Cells were washed three times with phosphate buffered saline solution (PBS) prior to imaging.

Optical trapping and single particle Raman

Combined Raman-optical tweezer studies were carried out using a previously described setup.[23, 24] The Raman tweezers apparatus consists of a cw Verdi V8 (Coherent) with laser beam wavelength of 532 nm and maximum power of 8 W. The beam is passed through two sets of expansion optics, reflected from Semrock razoredge dichroic mirror (LPD532-1) and directed into the microscope. A second dichroic mirror reflected the beam through the objective lens (63×, NA 1.2, Leica Microsystems) where the optical trap is formed. For trapping and acquisition of Raman spectra the laser was attenuated to a power of 16 mW, measured at the entrance aperture of the objective lens, yielding approximately 5 mW at the objective output.

The Raman light scattered from the focal point was collimated by the objective lens and passed back along the same optical pathway. A Semrock edge filter was placed after the razoredge to transmit only the Raman shifted light above 532 nm. The beam was then focussed onto the entrance slit of a spectrometer (SpectraPro-2500i, Acton Research Company) and detector (Spec-10:400B, Princeton Instruments). To allow observation of trapped particles, filtered light (>700 nm) from the microscope is used to image the particle onto a CCD camera. Calibration of the spectrometer was performed using liquid toluene (Spectroscopic grade, Aldrich) as a standard. Recorded wavenumbers were accurate to within 2 rel. cm^{-1}. Raman spectra and trapping of carbon microspheres were recorded using capillary tubes to minimize thermal effects. Raman spectra of carbon particles were baseline subtracted using a spectrum of the background medium collected during the same measurement run. Spectra thus obtained were fitted to a Breit-Wigner-Fano line for the G peak, a Gaussian curve for the D peak[25] and a polynomial to remove any residual background using data analysis software (Igor Pro).

Confocal microscopy

High-resolution confocal images were obtained using a Nikon confocal laser scanning microscope, EC1-Si (CLSM) attached to an inverted Nikon TE2000-U microscope and a 60× water immersion objective (NA 1.2). For imaging carbon microspheres in cells particles functionalised with 6-aminofluorescein (FL-LiDCA) were used in combination with DiI as a cellular membrane probe. An argon ion and a helium-neon laser operating at 488 and 543 nm, respectively, were used alternately with line switching using the multi-track facility of the CLSM. Images were collected using a 488/543 dichroic beam splitter and a 512-530 band pass filter (channel 1) to detect fluorescence from FL-LiDCA particles, using a 560-615 band pass filter to detect fluorescence from the DiI membrane probe (channel 2) and using optical white light transmission (channel 3).

Results and Discussion

Carbon microsphere characterization

Porous carbon spheres were synthesised via ultraspray pyrolysis from aqueous precursor solutions of dichloroacetates at 700 °C, following methods developed by Skrabalak et al.[18] This method allowed for the preparation of carbon particles using a continuous synthesis approach that is inherently scalable. Figures 1a and 1b show scanning electron microscopy (SEM) images of microspheres prepared using lithium and sodium dichloroacetate (LiDCA and NaDCA) respectively as organic precursors. The particles were found to be spherical in nature and the morphology of these particles depends on the precursor used. In agreement with previous reports,[18] Brunauer-Emmett-Teller (BET) analysis showed that LiDCA particles had higher specific surface areas than NaDCA particles, yielding values of 1043 m^2/g and 545 m^2/g, respectively. Barrett−Joyner−Halenda (BJH)[21] pore analysis yielded pore diameters in the mesopore range[22] at 3.4 nm and 32 nm for LiDCA and NaDCA, respectively. Figure 1c shows size distributions obtained from SEM images for the carbon samples used in our experiments. The distributions have a geometric mean of 689 nm and 1583 nm for LiDCA and NaDCA, respectively, and a geometric standard deviation of 35 %.

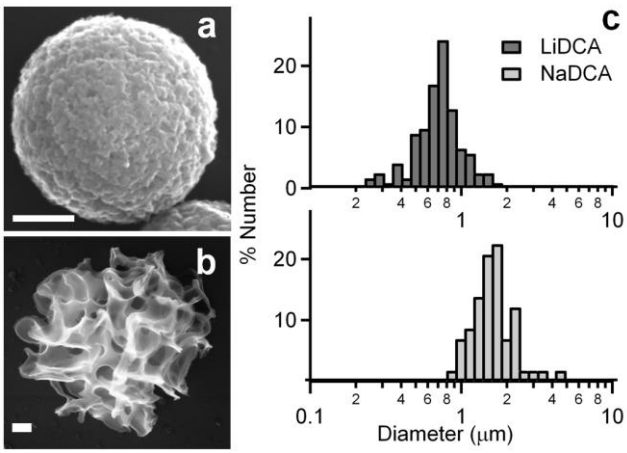

Fig. 1 Scanning Electron Microscopy (SEM) images (scalebar = 200 nm) of carbon spheres synthesized via ultraspray pyrolysis using aqueous solutions of Lithium (a) and Sodium (b) dichloroacetate as organic precursors. (c) size distributions of LiDCA and NaDCA particles used in our experiments.

Figure 2a shows a representative infrared transmission spectrum of microspheres used in our experiments. The infrared spectrum shows broad absorptions in the region 1700-1000 cm^{-1} characteristic of disordered graphitic carbons such as soots and carbon blacks. A prominent broad and intense contribution around 1600 cm^{-1} can be assigned to C—C stretching modes of polyaromatic systems and suggests that microparticles consist mainly of sp^2 carbon.[26, 27]

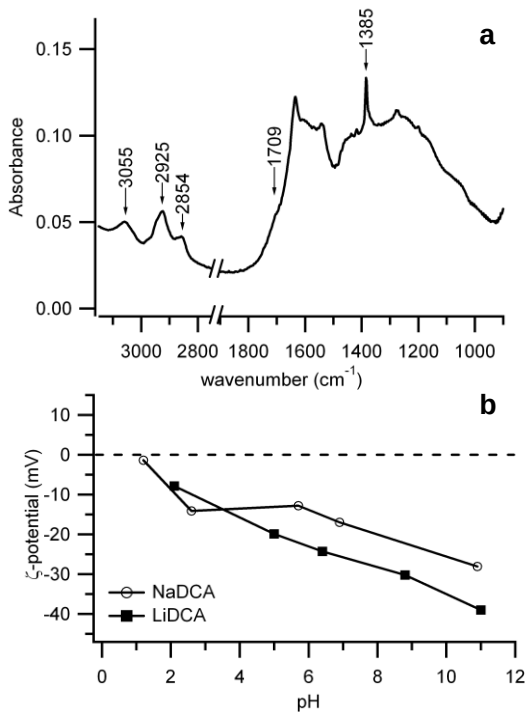

Fig. 2 (a) Infrared transmission spectrum of carbon microspheres; (b) ζ-potential of carbon microspheres in aqueous suspensions as a function of pH.

This conclusion is supported by the presence of an aromatic C—H stretching peak at 3055 cm^{-1} [28] and by Raman spectroscopic characterization of the microspheres (vide infra). The presence of aliphatic C—H stretching modes at 2854 and 2925 cm^{-1} and of methyl bending modes at 1385 cm^{-1} indicate that microspheres also contain residual sp^3 carbon after thermal decomposition of the organic precursor.[28] Finally, the infrared spectrum in Figure 2a shows a shoulder at 1709 cm^{-1} that can be assigned to the C=O stretching mode of carboxylic acid groups (—COOH).[26-28] FTIR results suggest that acid groups, which can impart a negative surface charge to the microspheres, are likely present on the carbon surface after synthesis. The presence of carboxylic groups was further supported by ζ-potential measurements of pristine particles in aqueous suspensions, which yielded negative ζ-potential values over the 2-10 pH range. Figure 2b shows the ζ-potential of microspheres as a function of pH from which an estimated isoelectric point of pH_{iep} = 0.2 and 1.0 for LiDCA and NaDCA particles, respectively, was determined. Values of pH_{iep} < 2 are frequently observed for black carbons after mild activation treatment,[29] and confirm that negatively charged groups are present on the particle surface under the pyrolysis conditions used for the synthesis.

Raman-optical tweezer studies of carbon microspheres

Raman-optical tweezer studies were carried out in order to determine the optical properties of carbon microspheres. Carbon microspheres in suspension were optically trapped and tracked in real time in a combined Raman-optical tweezer setup (λ_{exc} = 532 nm, incident power 5 mW for all reported experiments). Individual particles could be either trapped in solution or pinned against the glass walls of the sample holder. Once in the optical trap, particles could be observed over prolonged times while simultaneously collecting Raman spectra, thus allowing the investigation of the behaviour of isolated particles. Figure 3 shows the background-subtracted spectrum of a single microsphere in deionized water. The spectrum displays two peaks with maxima at 1597 and 1341 rel. cm^{-1} that are assigned to the G and D peaks respectively of amorphous carbon.[25, 30] The I(D)/I(G) height ratio is a useful parameter for determining the degree of order in amorphous carbons[25] and for our particles it was found to have a value of 0.61 ± 0.09. Based on the model developed by Robertson and co-workers[25] for the interpretation of Raman spectra of carbons, a G peak position of 1597 cm^{-1} and I(D)/I(G) = 0.61 suggest that the sp^2 content in these carbon microspheres is >80%.

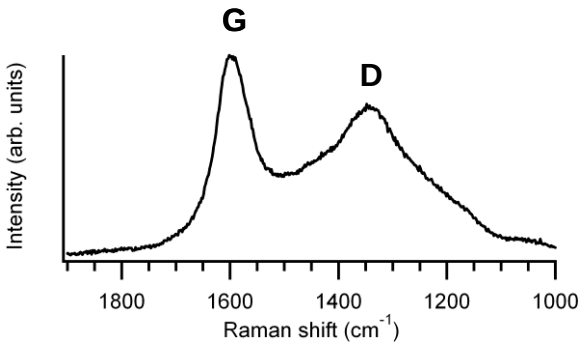

Fig. 3 Raman spectrum of an individual LiDCA particle in water.

We carried out Raman-trapping experiments of single particles in a wide range of solvents and observed significantly different

behaviour. Single carbon particles suspended in water and ethylene glycol could be trapped and held for several minutes without observing any changes in their spectral signature (see Supporting Information); however, when particles were suspended in octanol and N,N-dimethylformamide (DMF) we observed intense and broad visible emission almost immediately after trapping. No significant difference was observed in this behaviour between LiDCA and NaDCA spheres. An example of a single particle emission event is shown in Figure 4a.

When the emission contribution does not saturate the signal, it is possible to monitor in real time the evolution of the carbon Raman spectrum. Figure 4b shows Raman spectra of a single particle trapped in octanol collected over 16 s; Figure 4c shows the difference Raman spectrum obtained by subtracting the octanol scattering contribution from spectra reported in Figure 2b. Raman difference spectra show that, as the particle resides in the optical trap, its Raman spectrum evolves significantly. First, the I(D)/I(G) ratio increases visibly from 0.56 to 2.2; second, both the G and D peak maxima shift to lower values by up to ~20 cm-1 before returning close to their original positions. This behaviour is in contrast to results obtained in water, where the carbon Raman spectrum remains unchanged over long times under the same conditions.

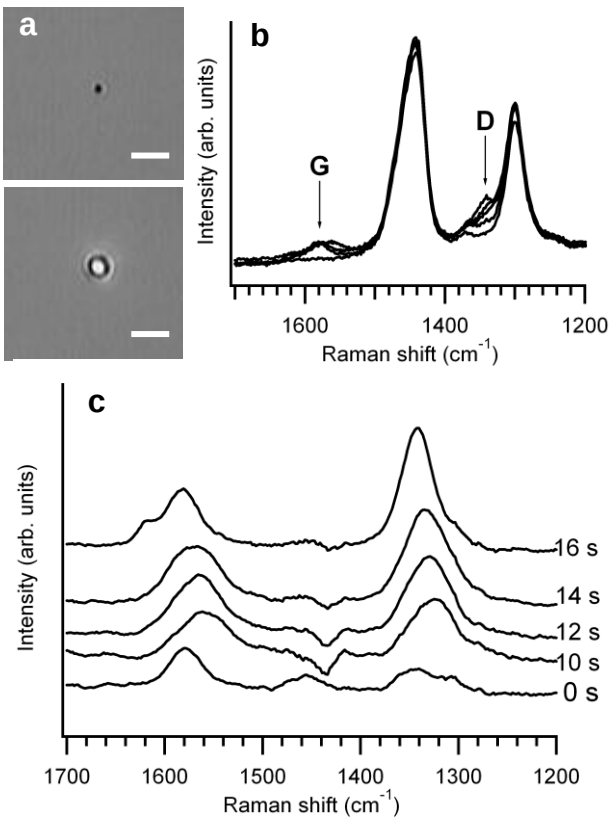

Fig. 4 (a) Image of a single LiDCA particle before and after being optically trapped in octanol (scalebar = 5 μm). (b) Spectral changes displayed by a single carbon sphere in octanol monitored over 16 s; the intense peaks at 1440 and 1300 cm^{-1} arise from the octanol contribution. (c) Raman of the carbon particle obtained by subtraction of the octanol background from spectra in (b); spectra have been smoothed and offset for the sake of clarity.

The increase in I(D)/I(G) ratio and the shift in peak position strongly suggest that carbon particles undergo annealing while in the optical trap. In amorphous carbons the development of a D peak is indicative of progressive ordering (opposite to what is found in graphite).[25] Both experimental data and theoretical models show that an increase in the height in I(D)/I(G) ratio accompanies thermal annealing and follows graphitization and ordering.[25, 31-33] The spectral shift of D and G maxima is also consistent with thermal annealing of the particles since an increase in temperature is known to lower the phonon frequencies in disordered carbons[34, 35] due to anharmonic effects and thermal expansion.[36] Temperature coefficients for the G mode of ordered forms of carbon and carbon black are reported to be in the range of -0.015 to 0.025 cm^{-1}/K.[37-39] Therefore, a 20 cm^{-1} downshift is suggestive of a significant increase in temperature which, assuming a constant value for the temperature coefficient, approximate to 800 K. Such temperatures if present should be sufficient to induce structural ordering and indicate that carbon particles are heated to high temperatures sufficient to cause an increase in graphitic content.

The emission observed upon trapping in organic solvents on both the Raman spectrum and the capture camera could originate from both photoluminescent[12, 40] and incandescent[41] behaviour of the particles. Although carbon nanoparticles have been shown to display visible photoluminescence, there are no reports of carbon microparticle photoluminescence. Control experiments carried out with particles in solution and on glass surfaces showed that neither pristine LiDCA nor NaDCA particles display fluorescent behaviour (see Supporting Information). We therefore attribute the origin of the bright emission shown in Figure 4a to particle incandescence generated by an increase in particle temperature.

Absorption of light from the incident laser is known to cause heating of carbon particles to the point of incandescence; this phenomenon is known as laser-induced incandescence (LII). LII has historically been used to characterise combustion aerosols using pulsed lasers,[41-44] but has been observed only recently for particles in liquid suspensions.[45] The ability to observe incandescence depends on whether the absorbed energy can be dissipated at a sufficiently high rate and therefore depends on numerous factors: particle surface/volume ratio, heat conductivity of the surroundings, laser flux and the occurrence of chemical reactions and phase changes.[44] In our case, we did not observe qualitative differences in emission between particles of different specific surface area. On the other hand, we observed marked differences when single particles were trapped in various solvents: no emission was observed in water and ethylene glycol whereas immediate intense emission was seen in DMF and octanol. These differences can be explained by considering the thermal conductivities of water, ethylene glycol, DMF and octanol which are 0.6071, 0.256, 0.184 and 0.161 W K^{-1} m^{-1} (at 298 K) respectively.[46] At constant incident laser irradiance it is easier to observe emission for suspensions prepared with solvents that display poor heat conduction, indicating that emissive behaviour, under our experimental conditions, is dominated by the heat conductivity properties of the surrounding medium. This is consistent with recent observations by Natarajan *et.al.* who observed a similar dependence of incandescent phenomena for carbon nanotubes in gaseous environments of different heat conductivity.[47]

In order to test this hypothesis we investigated whether it was possible to obtain emission in good dissipating media such as water by changing the heat conductivity properties of the particle surroundings. We prepared aqueous solutions of the cationic lipid, N-[1-(2,3-Dioleoyloxy)propyl]-N,N,N-trimethylammonium methylsulfate (DOTAP) at 0.04%, and of the anionic surfactant sodium dodecyl sulfate (SDS) at 1% and performed Raman-tweezer studies on suspended carbon microspheres. We observed that, although it was possible to trap carbon spheres in both surfactant solutions, we could obtain single particle emission only when using DOTAP. Similarly, particle annealing was observed only in DOTAP aqueous solutions. Figure 5a shows typical changes in the Raman signature observed for an individual particle as a function of time spent in the optical trap in 0.04% DOTAP; the I(D)/I(G) ratio increases as a function of time as in the case of octanol suspensions. The plot in Figure 5b summarizes the evolution of I(D)/I(G) ratios as a function of time spent in the optical trap for NaDCA particles in aqueous solutions of DOTAP and SDS. Under the same measurement conditions there is a marked increase in the I(D)/I(G) ratio in DOTAP but not in SDS solutions after prolonged trapping. This suggests that carbon particles are heated to higher temperatures when using the cationic surfactant whereas heat dissipation occurs more readily in SDS solutions.

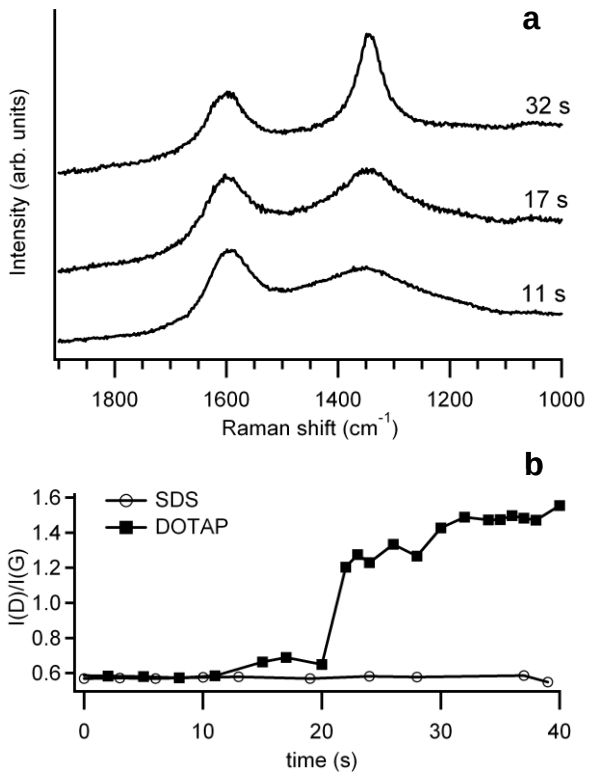

Fig. 5 (a) Changes in the Raman spectrum over a 20 s time interval for NaDCA spheres held in the optical trap in aqueous DOTAP solutions. (b) I(D)/I(G) ratio of the carbon Raman peaks of NaDCA spheres held in the optical trap in aqueous solutions of DOTAP and SDS surfactants.

The adsorption of ionic surfactants on solid surfaces is a complex process that results from a balance of electrostatic and hydrophobic interactions. It is known that surfaces that possess both hydrophobic and anionic sites (e.g. cellulose, activated carbons), as in the case of our particles, display higher adsorption rates and sorption capacity for cationic surfactants than for anionic surfactants.[48-51] DOTAP is therefore expected to adsorb more readily on carbon microspheres than SDS, creating an organic-like environment and thus reducing the heat conductivity in the immediate vicinity of the particles to a greater extent.

Studies of carbon microspheres in cells

Our experiments in solution show that carbon spheres absorb light and display localized heating to high temperatures suitable for particle annealing and incandescent emission. Therefore, we decided to determine whether the properties of these particles could be exploited in cellular uptake studies. The behaviour of particles was investigated using both human embryonic kidney (HEK293) and human epithelial carcinoma (HeLa) cells. Cells were incubated in the presence of particles for 12 h at 37 °C using the cationic transfection agent FuGENE® to aid cellular uptake. Confocal microscopy was used to gain insights into the location of particles within the cell. These measurements were carried out on cells incubated with fluorescently labelled LiDCA particles (FL-LiDCA), prepared via amide coupling of 6-aminofluorescein (FL-NH_2) to -COOH surface groups using previously reported procedures.[19] Multiple cycles of washing and centrifugation were necessary to ensure the removal of any physisorbed dye because of the high porosity of these microspheres. The washing process was repeated until no emission from the fluorescein dye was detectable in the supernatant solution upon excitation at 480 nm (pH 7). Figure 6 shows the photoemission spectra of LiDCA carbon particles before and after labelling with 6-aminofluorescein; the emission from the particle supernatant is reported for comparison. DiI was used as a membrane stain to allow resolution of the cell membrane. A complete depth profile (2 μm) of the cell was acquired by recording 30 scans at 150 nm intervals with separate particle (λ_{exc}=488 nm) and membrane dye excitation (λ_{exc} =543 nm).

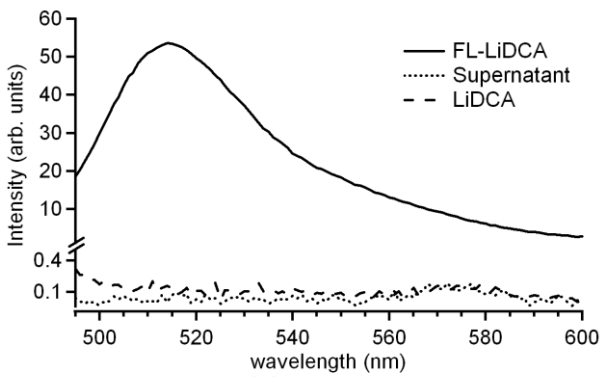

Fig. 6 Emission spectra of fluorescently labelled microspheres (FL-LiDCA), of the labelled particle supernatant, and of unlabelled microspheres (LiDCA), all recorded upon excitation at 480 nm in water at pH 7.

Fluorescein emission from dye molecules covalently linked to the particles is observed after incubation with both HEK293 and HeLa cells. Analysis of scan sequences show that particles appear

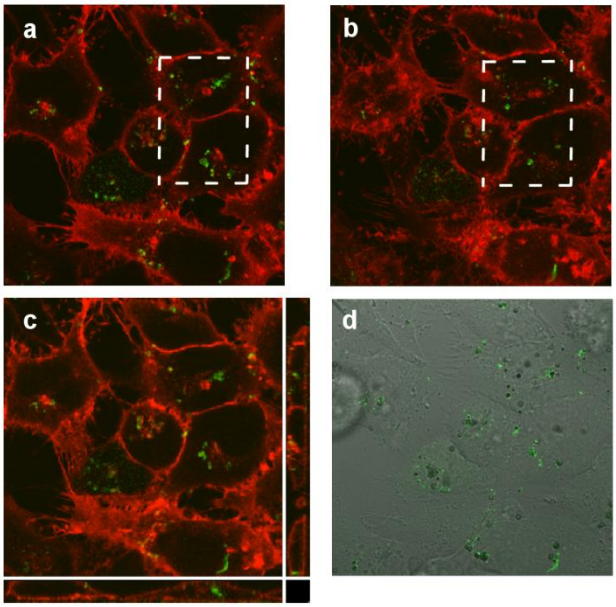

Fig. 7 Confocal images of HeLa cells after incubation with FL-LiDCA particles. (a) and (b) are sample scans showing changes in particle fluorescence with z-depth. (c) Z-scan rendering of carbon particle internalization in HeLa cells; the cell membrane is stained with DiI. and (d) Transmission image showing fluorescent nanoparticles

and subsequently disappear upon progression through the cell. A typical example is shown in Figure 7, where images (a) and (b) are recorded 900 nm apart and the presence of the particles in the highlighted area is seen to change significantly. The z-travel distance required to observe disappearance/appearance correlated well with the ~700 nm average size of the particles. Figure 7c shows a Z-scan rendering of images collected for both emission channels; the rendering indicates that particles are distributed within the cytoplasm and are thus internalised by the cells. Figure 7d shows the transmission image overlayed with the fluorescence image for the fluorescein channel. Strong fluorescence was typically observed over the capture size of 78 μm^2; this suggests that particles are preferentially clustered in specific subcellular structures. These results indicate that carbon particles are uptaken by both cell lines and that molecules covalently linked to the surface of the microspheres, in our case a fluorescent dye, can be successfully delivered to the cytoplasm. The most likely mechanism for particle uptake is endocytosis which has been observed for similarly sized particles.[52] In our studies particle uptake was not seen to compromise cell viability and both cell lines remained viable for several days with normal cell division.

Having observed laser-induced incandescence in solution we were interested in investigating whether the behaviour would persist in the cell environment. Optical trapping experiments were therefore repeated on cells incubated in the presence of NaDCA and LiDCA particles. It was possible to trap and manipulate particles located both at the cell surface and within the cytoplasm, while at the same time obtaining their carbon Raman spectra. Once in the optical trap, particles were found to display incandescence in a similar fashion to that observed in the presence of DOTAP. Furthermore, in cases where the particle was located near to the cell membrane the induced incandescence resulted in blebbing and membrane rupture. This is shown to dramatic effect in Figure 8a-f, for the case of a carbon particle located adjacent to the membrane of a HeLa cell. The particle displays bright incandescence (b) which results in a disturbance that propagates around the whole cell over a few seconds (c-h). In other cases the incandescence resulted in complete membrane rupture with loss of intracellular material and cell death. Membrane rupture was also accompanied by changes in the carbon Raman signature, similar to those observed in media of poor heat conductivity indicating that carbon annealing and graphitization takes place also within cells. Importantly, no cell damage was observed due to the incident laser alone under the same conditions.

Conclusions

In this work we have used Raman and optical trapping to demonstrate that absorption of 532 nm laser light by individual carbon mesoporous microspheres causes dramatic changes in the particle temperature that are sufficient to induce graphitization

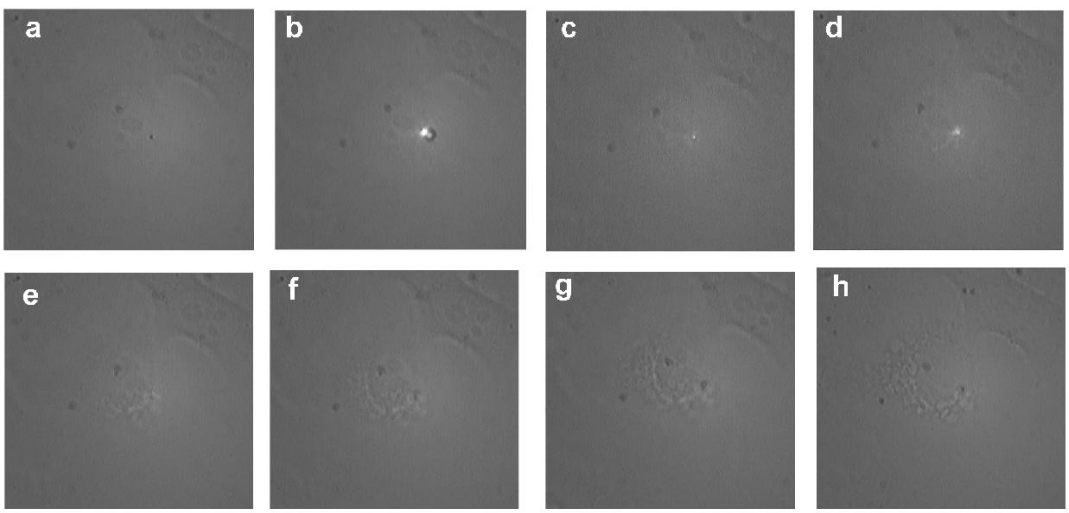

Fig. 8 Optical microscope image of a HeLa cell incubated with LiDCA particles (a) before, (b) during and (c = 0.5 s; d= 1.0 s; e = 2 s; f = 3 s; g = 9 s; h=10 s) after incandescent behaviour.

and incandescent emission. We have shown that this behaviour is related to the ability of the environment that surrounds the microparticle to dissipate heat. We have also demonstrated that particles are successfully uptaken by cells using a commercial transfection agent. Particles bearing small molecules covalently linked to their surface can be carried by the carbon scaffold into the cytoplasm, thus opening the possibility of using these particles for delivery applications. Furthermore we have shown that when introduced in the cellular environment light absorption by particles can trigger membrane disruption and cell death. In summary, these results demonstrate that it is possible to leverage two important characteristics of mesoporous carbon materials: their ability to deliver small molecules to the cytoplasm and their high optical absorptivity. The high specific surface area of these mesoporous carbon microspheres suggests that they are an excellent platform for the development of delivery agents with potential for temperature-activated release of bioactive compounds or materials. The ability to remotely initiate temperature-activated processes opens the possibility of therapeutic applications involving controlled cell damage.

Acknowledgements

This work was carried out at the Central Laser Facility, STFC Rutherford Appleton Laboratory. This publication has emanated from research conducted with the financial support of Science Foundation Ireland under Grant Number 10/RFP/CAP2915. We are grateful to EPA Ireland grant 2008-PhD-WRM-2.

Notes and references

[a] *School of Chemistry ,Trinity College Dublin, Dublin 2, Ireland Fax: 353 1 671 2826; Tel: 353 1 896 3562; Email: colavitp@tcd.*
[b] *School of Chemistry and Chemical Biology, Centre for Synthesis and Chemical Biology, University College Dublin, Dublin 4, Fax: 353 1 716 1178; Tel: 353 1 716 2407; E-mail: susan.quinn@ucd.ie*
[c] *Central Laser Facility, Research Complex at Harwell, Science & Technology Facilities Council, Rutherford Appleton Laboratory, Didcot, Oxfordshire, OX11 0QX, UK*

† Electronic Supplementary Information (ESI) available: [details of any supplementary information available should be included here]. See

DOI: 10.1039/b000000x/

1. L. Pasqua, S. Cundari, C. Ceresa and G. Cavaletti, *Curr. Med. Chem.*, 2009, **16**, 3054.
2. S. P. Rigby, M. Fairhead and C. F. van der Walle, *Curr. Pharm. Des.*, 2008, **14**, 1821.
3. B. G. Trewyn, Slowing, II, S. Giri, H. T. Chen and V. S. Y. Lin, *Acc. Chem. Res.*, 2007, **40**, 846.
4. S. H. Tang, X. Q. Huang, X. L. Chen and N. F. Zheng, *Adv. Funct. Mater.*, 2010, **20**, 2442.
5. A. M. Spokoyny, D. Kim, A. Sumrein and C. A. Mirkin, *Chem. Soc. Rev.*, 2009, **38**, 1218.
6. S. E. Rodil, R. Olivares, H. Arzate and S. Muhl, in *Carbon: The Future Material for Advanced Technology Applications*, 2006, pp. 55.
7. R. K. Roy and K. R. Lee, *J. Biomed. Mater. Res., Part B*, 2007, **83B**, 72.
8. B. Sun, P. E. Colavita, H. Kim, M. Lockett, M. S. Marcus, L. M. Smith and R. J. Hamers, *Langmuir*, 2006, **22**, 9598.
9. W. S. Yang, O. Auciello, J. E. Butler, W. Cai, J. A. Carlisle, J. Gerbi, D. M. Gruen, T. Knickerbocker, T. L. Lasseter, J. N. Russell, Jr., L. M. Smith and R. J. Hamers, *Nat. Mater.*, 2002, **1**, 253.
10. F. Liang and B. Chen, *Curr. Med. Chem.*, 2010, **17**, 10.
11. V. Krishna, N. Stevens, B. Koopman and B. Moudgil, *Nat. Nanotechnol.*, 2010, **5**, 330.
12. S. C. Ray, A. Saha, N. R. Jana and R. Sarkar, *J. Phys. Chem. C*, 2009, **113**, 18546.
13. A. S. Barnard, *Analyst*, 2009, **134**, 1751.
14. O. Faklaris, V. Joshi, T. Irinopoulou, P. Tauc, M. Sennour, H. Girard, C. Gesset, J. C. Arnault, A. Thorel, J. P. Boudou, P. A. Curmi and F. Treussart, *ACS Nano*, 2009, **3**, 3955.
15. M. Chen, E. D. Pierstorff, R. Lam, S. Y. Li, H. Huang, E. Osawa and D. Ho, *ACS Nano*, 2009, **3**, 2016.
16. Y. Fang, D. Gu, Y. Zou, Z. X. Wu, F. Y. Li, R. C. Che, Y. H. Deng, B. Tu and D. Y. Zhao, *Angew. Chem., Int. Ed.*, 2010, **49**, 7987.
17. T. W. Kim, P. W. Chung, Slowing, II, M. Tsunoda, E. S. Yeung and V. S. Y. Lin, *Nano Lett.*, 2008, **8**, 3724.
18. S. E. Skrabalak and K. S. Suslick, *J. Am. Chem. Soc.*, 2006, **128**, 12642.
19. G. T. Hermanson, *Bioconjugate Techniques*, Academic Press, Amsterdam, 2008.
20. S. Brunauer, P. H. Emmett and E. Teller, *J. Am. Chem. Soc.*, 1938, **60**, 309.
21. E. P. Barrett, L. G. Joyner and P. P. Halenda, *J. Am. Chem. Soc.*, 1951, **73**, 373.
22. K. S. W. Sing, D. H. Everett, R. A. W. Haul, L. Moscou, R. A. Pierotti, J. Rouquerol and T. Siemieniewska, *Pure Appl. Chem.*, 1985, **57**, 603.
23. T. J. Harvey, E. C. Faria, A. Henderson, E. Gazi, A. D. Ward, N. W. Clarke, M. D. Brown, R. D. Snook and P. Gardner, *J. Biomed. Opt.*, 2008, **13**, 064004.
24. J. M. Sanderson and A. D. Ward, *Chem. Commun.*, 2004, 1120-1121.
25. A. C. Ferrari and J. Robertson, *Phys. Rev. B*, 2000, **61**, 14095-14107.
26. M. S. Akhter, A. R. Chughtai and D. M. Smith, *Appl. Spectrosc.*, 1985, **39**, 143.
27. D. M. Smith and A. R. Chughtai, *Colloids Surf. A*, 1995, **105**, 47-77.
28. G. Socrates, *Infrared and Raman characteristic group frequencies. Tables and Charts*, John Wiley & Sons, Chichester, 2001.
29. C. Moreno-Castilla, M. A. Ferro-Garcia, J. P. Joly, I. Bautista-Toledo, F. Carrasco-Marin and J. Rivera-Utrilla, *Langmuir*, 1995, **11**, 4386.
30. J. Robertson, *Mat. Sci. Eng. R*, 2002, **37**, 129.
31. M. Chhowalla, A. C. Ferrari, J. Robertson and G. A. J. Amaratunga, *Appl. Phys. Lett.*, 2000, **76**, 1419.
32. A. C. Ferrari, B. Kleinsorge, N. A. Morrison, A. Hart, V. Stolojan and J. Robertson, *J. Appl. Phys.*, 1999, **85**, 7191.
33. M. A. Tamor and W. C. Vassel, *J. Appl. Phys.*, 1994, **76**, 3823-3830.
34. N. J. Everall, J. Lumsdon and D. J. Christopher, *Carbon*, 1991, **29**, 133.
35. E.-P. Huang, E. Huang, S.-E. Yu, Y. Chen, -H., J.-S. Lee and J.-N. Fang, *Phys. Chem. Miner.*, 2010, **37**, 593.
36. C. Postmus and J. R. Ferraro, *Phys. Rev.*, 1968, **174**, 983.
37. I. Calizo, A. A. Balandin, W. Bao, F. Miao and C. N. Lau, *Nano Lett.*, 2007, **7**, 2645.
38. F. M. Huang, K. T. Yue, P. H. Tan, S. L. Zhang, Z. J. Shi, X. H. Zhou and Z. N. Gu, *J. Appl. Phys.*, 1998, **84**, 4022.
39. P. H. Tan, Y. M. Deng, Q. Zhao and W. C. Cheng, *Appl. Phys. Lett.*, 1999, **74**, 1818.
40. A. B. Bourlinos, A. Stassinopoulos, D. Anglos, R. Zboril, V. Georgakilas and E. P. Giannelis, *Chem. Mater.*, 2008, **20**, 4539.
41. R. W. Weeks and W. W. Duley, *J. Appl. Phys.*, 1974, **45**, 4661.
42. A. C. Eckbreth, *J. Appl. Phys.*, 1977, **48**, 4473.
43. L. A. Melton, *Appl. Opt.*, 1984, **23**, 2201.
44. H. A. Michelsen, *J. Chem. Phys.*, 2003, **118**, 7012.
45. R. Sommer and A. Leipertz, *Opt. Lett.*, 2007, **32**, 1947.
46. in *CRC Handbook of Physical Constants*, ed. D. R. Lide, CRC Press, 1998, pp. 6.
47. S. Natarajan, Z. H. Lim, G. Wee, S. G. Mhaisalkar, C. H. Sow and G. W. Ho, *Scr. Mater.*, 2011, **64**, 564.
48. C. A. Basar, A. Karagunduz, B. Keskinler and A. Cakici, *Appl. Surf. Sci.*, 2003, **218**, 170.
49. S. Paria and K. C. Khilar, *Adv. Colloid Interface Sci.*, 2004, **110**, 75.
50. S. Paria, C. Manohar and K. C. Khilar, *Ind. Eng. Chem. Res.*, 2005, **44**, 3091.
51. T. F. Tadros, *J. Colloid Interface Sci.*, 1974, **46**, 528-540.

52. J. Rejman, V. Oberle, I. S. Zuhorn and D. Hoekstra, *Biochem. J.*, 2004, **377**, 159.

5